nature nanotechnology

LETTERS

PUBLISHED ONLINE: 13 JULY 2015 | DOI: 10.1038/NNANO.2015.135

Large anelasticity and associated energy dissipation in single-crystalline nanowires

Guangming Cheng[1†], Chunyang Miao[2,3†], Qingquan Qin[1], Jing Li[4], Feng Xu[1], Hamed Haftbaradaran[2], Elizabeth C. Dickey[4], Huajian Gao[2*] and Yong Zhu[1,4*]

Anelastic materials exhibit gradual full recovery of deformation once a load is removed, leading to dissipation of internal mechanical energy[1]. As a consequence, anelastic materials are being investigated for mechanical damping applications. At the macroscopic scale, however, anelasticity is usually very small or negligible, especially in single-crystalline materials[2,3]. Here, we show that single-crystalline ZnO and p-doped Si nanowires can exhibit anelastic behaviour that is up to four orders of magnitude larger than the largest anelasticity observed in bulk materials, with a timescale on the order of minutes. *In situ* scanning electron microscope tests of individual nanowires showed that, on removal of the bending load and instantaneous recovery of the elastic strain, a substantial portion of the total strain gradually recovers with time. We attribute this large anelasticity to stress-gradient-induced migration of point defects, as supported by electron energy loss spectroscopy measurements and also by the fact that no anelastic behaviour could be observed under tension. We model this behaviour through a theoretical framework by point defect diffusion under a high strain gradient and short diffusion distance, expanding the classic Gorsky theory. Finally, we show that ZnO single-crystalline nanowires exhibit a high damping merit index, suggesting that crystalline nanowires with point defects are promising materials for energy damping applications.

Nanowires exhibit a host of novel properties that are being exploited for many applications, including energy harvesting and storage[4,5], flexible/stretchable electronics[6,7], sensing[8] and nanoelectromechanical systems[9]. The vast majority of research on the mechanical properties of nanowires has focused on the size-dependent elastic modulus and strength[10–14], with very few studies on time-dependent responses[15,16]. Our single-crystalline nanowires exhibit an unexpectedly large anelastic relaxation and energy dissipation under bending.

Bending tests were performed at room temperature using a microelectromechanical system (MEMS)-based nanomechanical testing stage inside a scanning electron microscope (SEM; Fig. 1a)[17,18]. After holding the nanowire in a bent configuration for a certain time (the 'holding time'), the MEMS actuator was retracted and the shape of the nanowire was monitored in real time (Fig. 1b and Supplementary Movie 1). A large portion of the bending strain was observed to recover instantaneously, with the rest recovering gradually over time.

Figure 2a shows the evolution of the anelastic strain of a ZnO nanowire (54 nm in diameter) for an initial (total) bending strain of 1.94% with six different durations of holding time. Here, the initial or total strain is the sum of the anelastic strain and elastic strain, just before the load is removed. It can be seen that the recovery of the anelastic strain depends on the holding time—the shorter the holding time, the faster the recovery. Figure 2b shows the evolution of the anelastic strain for a holding time of 15 min under five different initial strains. A larger initial strain led to a larger anelastic strain. The anelastic strain recovered almost fully with time (see Supplementary Fig. 2a for an example with a holding time of 15 min and a recovery time of up to 40 min). The anelastic strain was as large as 0.64% (in the case of 4.1% total strain).

Five ZnO nanowires were tested, and all exhibited the same anelastic behaviour (Fig. 2c and Supplementary Fig. 2b,c). Figure 2d shows the maximum anelastic strain (immediately after removal of the load) as a function of initial strain for all tested ZnO nanowires. In general, the maximum anelastic strain scales nonlinearly with the initial strain, but for small initial strain, a linear approximation holds.

A number of anelastic mechanisms could be present in single-crystalline materials, including thermoelastic relaxation, piezoelectric coupling and relaxations involving point defect motion[1–3]. To elucidate the underlying mechanism(s), additional experiments were carried out with ZnO nanowires subjected to uniaxial tension and compression. Under tension, they exhibited a linear elastic behaviour without observable hysteresis (Fig. 2e)[19], but, under compression, they buckled and exhibited a strong hysteresis (Fig. 2f). The tension and compression tests were conducted using the same set-up, with the same mechanical/electrical boundary conditions and at loading rates comparable to the inverse timescale associated with the aforementioned relaxation under bending. Hence, relaxation occurs only under an inhomogeneous strain field (for example, bending or compression/buckling), rather than under a homogeneous strain field (for example, tension). Previously observed anelastic behaviour in GaAs nanowires was attributed to the amorphous/crystalline interface at the nanowire surface[15], but this could not account for the observed differences between bending and tension in our present study.

Two types of relaxation, thermoelastic and Gorsky relaxation, are known to operate under an inhomogeneous strain field[1]. Under thermoelastic relaxation, both the relaxation strength (amplitude) and relaxation time are much smaller than those observed in ZnO nanowires (Supplementary Section 3)[20]. It is therefore Gorsky relaxation, which arises from the motion of point defects in an inhomogeneous stress field[21,22], that is identified as a likely operating mechanism here. When a beam that contains volume-sensitive point defects (for example, interstitials or vacancies) is subject to

[1]Department of Mechanical and Aerospace Engineering, North Carolina State University, Raleigh, North Carolina 27695, USA. [2]School of Engineering, Brown University, Providence, Rhode Island 02912, USA. [3]Institute of Nano Science, Nanjing University of Aeronautics and Astronautics, Nanjing 210016, China. [4]Department of Materials Science and Engineering, North Carolina State University, Raleigh, North Carolina 27695, USA. †These authors contributed equally to this work. *e-mail: huajian_gao@brown.edu; yong_zhu@ncsu.edu

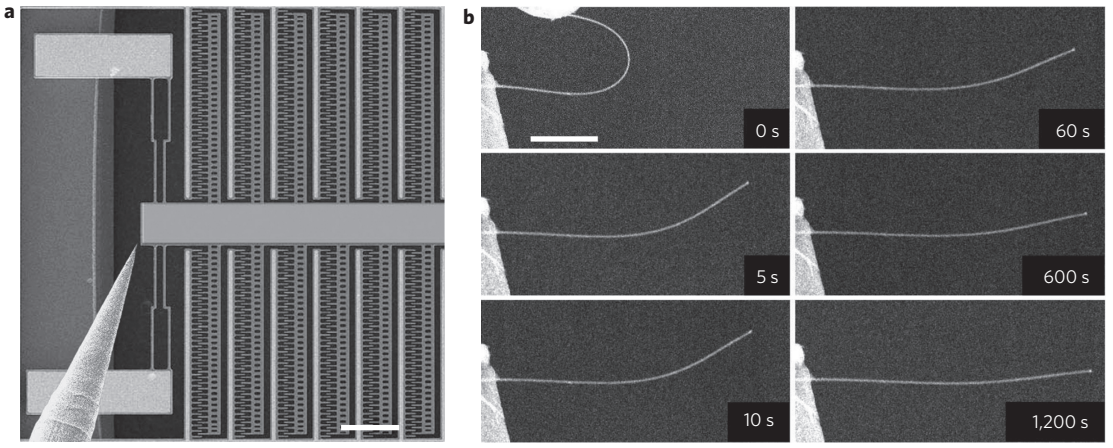

Figure 1 | *In situ* SEM bending test of an individual ZnO nanowire. a, Experimental set-up showing an individual ZnO nanowire bent between a MEMS stage (right) and a nanomanipulator tip (left). Scale bar, 100 μm. **b**, A sequence of SEM images showing the recovery process for a ZnO nanowire after removing the bending load. Scale bar, 2 μm.

bending, the stress gradient across the sample creates a gradient in chemical potential along which the point defects migrate. For example, long-range diffusion of interstitials goes from the compressed side to the dilated side, while vacancies migrate in the opposite direction. However, the classic Gorsky relaxation predicts a linear relationship between the maximum anelastic strain and the initial strain, and has only been observed in a few bulk materials with very small relaxation amplitude[21,22].

A theoretical model was therefore developed to understand the relationship between the diffusion of point defects and the measured anelastic behaviour. The governing equation for the time-dependent evolution of defect concentrations was derived (see Methods). Finite-element simulations were performed to simulate the bending and relaxation processes under the same conditions as in the experiments. A number of defect types with corresponding diffusivities and initial concentrations were considered. The evolution of the anelastic strain was calculated as functions of the initial strain and holding time and compared to the experimental results (Fig. 2). For a nanowire with a diameter of 54 nm, the best fitting identified two types of point defects with diffusivities of 1.9×10^{-14} and 1.5×10^{-15} $cm^2\ s^{-1}$, at initial defect concentrations of 1.26×10^{20} and 3.67×10^{20} cm^{-3}, respectively. Note that the fitting is not trivial, yet robust, as the model predictions using the same parameters were able to fit a wide range of experimental results with different durations of holding time and different initial strains (Fig. 2a,b). The model predicts that a faster species of point defects dominates the rapid relaxation in the beginning, and a slower species of point defects governs relaxation, with a larger time constant (Supplementary Fig. 4). Interestingly, it has been reported that two dominant types of point defects exist in ZnO, oxygen vacancy and zinc interstitial[23], which is consistent with our results. During relaxation, oxygen vacancies could diffuse from the tensile to the compressive side, while zinc interstitials diffuse in the opposite direction. Note that the diffusivities identified above are larger than those for bulk ZnO at room temperature. Possible reasons for this deviation include (1) surface-mediated bulk diffusion (in nanowires, a substantial fraction of atoms lie near free surfaces, with an atomic structure considerably different from that in the bulk)[10,24] and (2) reduced activation energy under ultrahigh stress (on the order of GPa)[25]. It is worth noting that the current knowledge on room-temperature diffusion of point defects in bulk ZnO, and more so in ZnO nanowires, is very limited[26]. The present experimental approach can be a useful way to investigate transport and equilibrium properties of point defects in nanomaterials.

To corroborate the conclusion that the anelastic behaviour results from the diffusion of point defects, a further investigation of the defect structures in ZnO nanowires was carried out. The transmission electron microscopy (TEM) image in Fig. 3a shows that the ZnO nanowires are uniform in diameter. The corresponding selected area electron diffraction (SAED) pattern (Fig. 3a, inset) indicates that the nanowires are single-crystalline wurtzite, with a growth direction along the ⟨0001⟩ axis, and the high-resolution TEM image in Fig. 3b shows no extended structural defects (for example, stacking faults or dislocations).

Aberration-corrected scanning transmission electron microscopy/electron energy loss spectroscopy (STEM/EELS) was used to investigate the stoichiometry of ZnO nanowires under bending. The diffusion of point defects across the diameter would lead to a difference in stoichiometry at the two sides of a bent wire (termed the 'inner side' and 'outer side' in the following). Here, an individual nanowire protruding from a TEM grid was bent into a loop. Five positions with different bending strains were chosen along the axial direction (Fig. 3c,d). The quantitative EELS results show that the atomic percentage of oxygen (that is, stoichiometry) is different at the inner and outer sides, with the outer side always richer in oxygen than the inner side. By contrast, in undeformed (straight) regions the inner side and outer side have nearly the same stoichiometry, as expected (Supplementary Section 6). The same phenomenon was observed in three additional nanowires with a similar bending geometry. The differences in oxygen atomic percentage between inner and outer sides for the selected points are shown in Fig. 3e. The largest difference in oxygen atomic percentage is at position 3 (~4.2 at%), which corresponds to the largest local bending strain (~2.9%). Figure 3f shows a nearly linear relationship between the difference in oxygen concentration and the bending strain and anelastic strain (following Fig. 2d). The EELS results suggest that, during relaxation, more oxygen vacancies diffuse from the tensile (outer) to the compressive (inner) side than zinc interstitials in the opposite direction, leading to a higher oxygen percentage in the outer side.

Two conditions are usually necessary for Gorsky relaxation: (1) the point defects must cause lattice distortion, which changes the volume of the host lattice; (2) they must have relatively high mobility. So far, Gorsky relaxation has only been observed in bulk samples with hydrogen (or its isotope) as the most mobile interstitial species[21,22], with anelastic strain less than 10^{-6}. The observed anelasticity in the present study is four orders of magnitude higher than the largest observed value at the macroscopic scale.

How can Gorsky relaxation lead to the observed large anelasticity in ZnO nanowires? Nanostructures can typically withstand

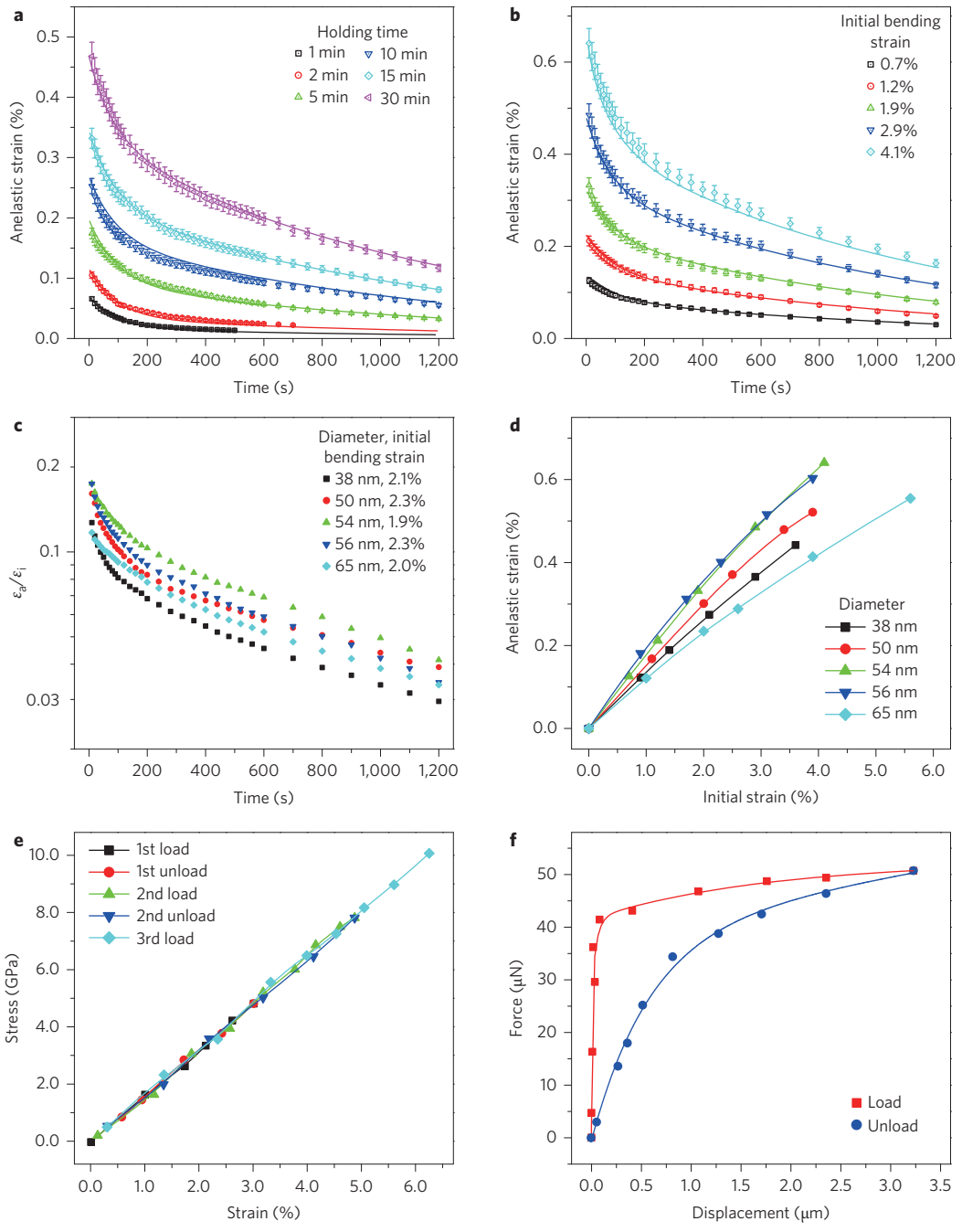

Figure 2 | Recovery and damping behaviours of a ZnO nanowire. a, Anelastic strain as a function of recovery time for six different durations of holding time for a nanowire with a diameter of 54 nm and an initial bending strain of 1.94%. **b**, Anelastic strain as a function of recovery time for five different initial bending strains. The holding time was 15 min in all cases. Solid lines in both **a** and **b** represent the fitting data from the theoretical analysis. Error bars for strain measurement in **a** and **b** are ~5.4%. **c**, Normalized anelastic strain (anelastic strain divided by elastic strain) as a function of recovery time for five ZnO nanowires with diameters of 38, 50, 54, 56 and 65 nm with the same holding time of 15 min. **d**, Maximum anelastic strain as a function of initial strain for the five ZnO nanowires. The holding time was 15 min in all cases. Note how, for larger initial strains, the relationship becomes nonlinear. **e**, Stress–strain curve for a ZnO nanowire under tension. **f**, Force–displacement curve for a ZnO nanowire under compression (buckling).

ultrahigh stress (on the order of GPa) or strain (on the order of a few per cent)[25]. In the present study, the bending strain in the ZnO nanowires is as large as 5.6% with stress over 8 GPa (ref. 19). By contrast, for hydrogen diffusion in bulk materials[21,22], the bending strain is usually less than 10^{-5}. The ultrahigh bending stress (strain) applied to the nanowire is responsible for the magnitude of the large anelastic strain. According to equation (S8) in Supplementary Section 4, the diffusional flux of point defects depends on the chemical potential gradient, which in turn depends on the stress gradient. The small diffusion distance (due to the small nanowire diameter), enormous stress gradient and the high diffusivity therefore contribute to the short relaxation (recovery) timescale (on the order of minutes).

It should be noted that our theoretical model is more general than the classic Gorsky theory. The classic Gorsky theory predicts a linear relationship between the initial strain and the anelastic strain, while our model predicts a nonlinear relationship when the strain is large. The relaxation phenomenon reported in the present study

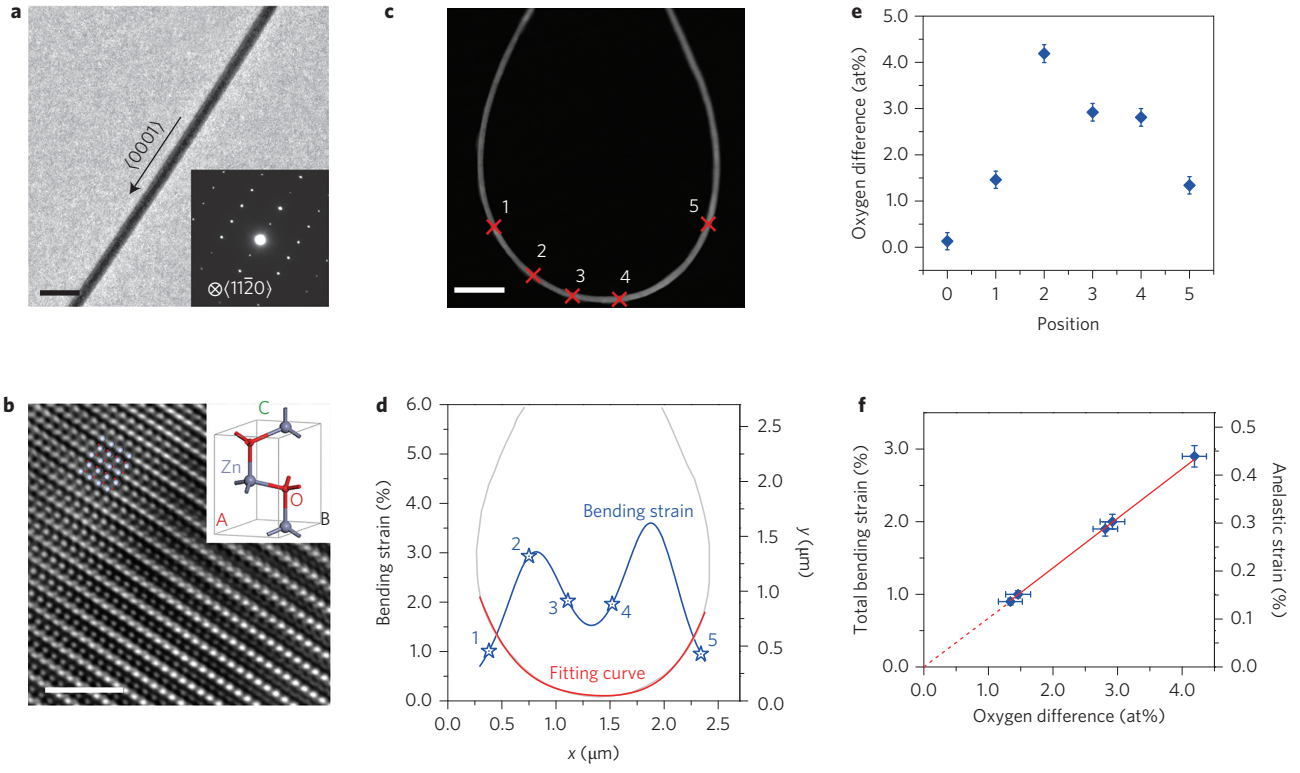

Figure 3 | Microstructure and relationship between oxygen difference and bending strain for a ZnO nanowire. a, Overview of an individual ZnO nanowire with a diameter of 37 nm and a growth direction of ⟨0001⟩. Inset: corresponding SAED pattern at the zone axis of ⟨11$\bar{2}$0⟩. Scale bar, 100 nm. **b**, High-resolutionTEM image showing a perfect atomic arrangement in the close-packed layers of {0001}. Inset: atomic model of a ZnO unit cell. Scale bar, 2 nm. **c**, High-angle annular dark-field (HAADF)-STEM image showing a bent nanowire for EELS analysis. Scale bar, 0.5 μm. **d**, Bending strain as a function of position in the bent ZnO nanowire. **e**, EELS analysis showing the difference in oxygen concentration between outer and inner sides of the bent ZnO nanowire at different positions. Position 0 was taken from a straight part with zero bending strain. Error bars are from the variation in stoichiometry (~0.5 at%). **f**, Linear relationship between the difference in oxygen concentration (between outer and inner sides) and the total bending strain and anelastic strain.

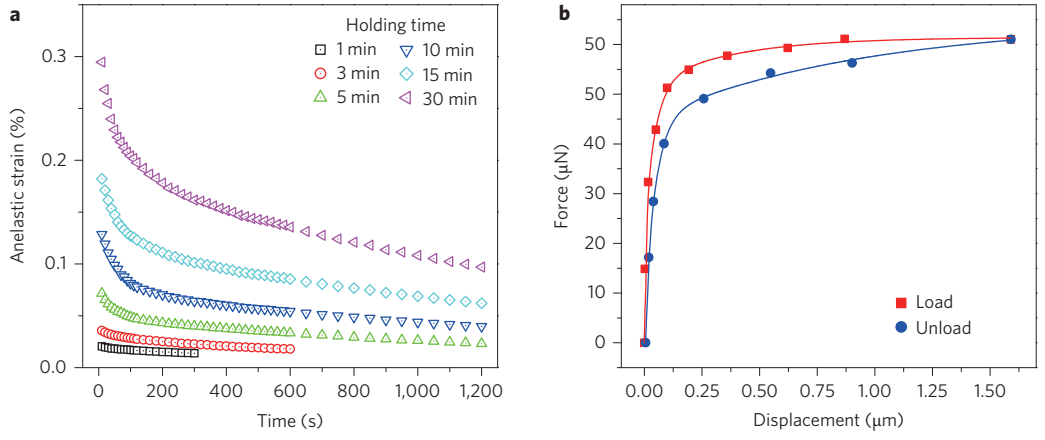

Figure 4 | Mechanical behaviour of p-doped Si nanowires under bending and compression. a, Anelastic strain as a function of recovery time for six different durations of holding time (initial strain 2.4%). **b**, Force–displacement curve of a p-doped Si nanowire under compression (buckling).

may therefore be referred to as a type of nonlinear Gorsky relaxation. As discussed in Supplementary Section 5, the Gorsky model is a special case of our theoretical model when there is only one type of diffusion species and the applied strain gradient is small.

Anelasticity can lead to energy dissipation (or internal friction), which is of great technological interest. Figure 2f shows the hysteretic behaviour of a ZnO nanowire under compression. Here, the energy dissipation can be characterized by the loss factor $\eta = \Delta W/\pi W_{max}$, where ΔW is the dissipated energy per loading–unloading cycle and W_{max} is the maximum stored energy per unit volume over the cycle. A high loss factor of ~0.08 is calculated from Fig. 2f. High-damping materials typically have low stiffness (Young's modulus)[27]. In load-bearing applications, however, both high stiffness and high damping are often desired. A merit index is given by $\sqrt{E}\eta$, where E is Young's modulus[28]. The merit index for the ZnO nanowire is remarkably high with a value of 1.13, giving $E = 200$ GPa for a diameter of 20 nm (ref. 19). For the purpose of comparison, among the bulk materials traditionally used as high-damping materials, Cu–Mn alloys exhibit the highest merit index of ~0.5. Recently, nanopillars made of

Cu–Al–Ni single-crystalline shape memory alloy were reported to have a merit index of ~0.9 (ref. 28). Clearly, the ZnO nanowires exhibit promising potential for mechanical damping and might be used as an efficient damping material in a broad range of applications.

To assess whether the observed anelasticity is present in other single-crystalline nanowires with point defects, we tested p-doped Si nanowires and observed similar anelastic relaxation. Figure 4a shows that the relaxation in p-doped Si nanowires is slower than that in ZnO nanowires for the same holding time, indicating slower diffusion of boron dopants in the Si nanowires (Supplementary Movie 2). Figure 4b plots the load–displacement curve of a Si nanowire under buckling, illustrating a similar hysteretic behaviour with a loss factor of ~0.025 and a merit index of 0.36. Preliminary tests on single-crystalline Ag nanowires showed anelastic behaviour at sufficiently small strains, but, at higher strains, dislocation activities induced plastic deformation, resulting in incomplete strain recovery.

In summary, we have reported large anelastic behaviour in single-crystalline nanowires governed by the stress-gradient-induced migration of point defects. The observed anelasticity was attributed to a type of nonlinear Gorsky relaxation that involves the diffusion of two types of point defect under an inhomogeneous stress field. The large anelasticity in ZnO nanowires resulted in high mechanical damping with a merit index of 1.13. Similar anelastic behaviour was found in p-doped Si nanowires. This effect is attributed to the high strain applied to the nanowires, while the small diffusion distance, enormous stress gradient and large diffusivity result in the short relaxation (recovery) timescale. The large diffusivity in nanowires is due to surface-mediated bulk diffusion and reduced activation energy under ultrahigh stress. The present study also suggests a useful experimental approach to study transport and equilibrium properties of point defects at the nanoscale. Because point defects have been reported to exist in many nanostructures[29], the reported anelasticity is expected to have broad impacts in nanotechnology. Thanks to the rapid progress in the large-scale synthesis of nanowires[30], we suggest that crystalline nanowires with point defects could serve as highly efficient damping materials for a broad range of applications in the aerospace, automotive, energy and biomedical industries.

Methods

Methods and any associated references are available in the online version of the paper.

Received 15 December 2014; accepted 1 June 2015; published online 13 July 2015

References

1. Lakes, R. *Viscoelastic Material* (Cambridge Univ. Press, 2009).
2. Zener, C. *Elasticity and Anelasticity of Metals* (Univ. Chicago Press, 1948).
3. Nowick, A. S. & Berry, B. S. *Anelastic Relaxation in Crystalline Solids* (Academic, 1972).
4. Wang, Z. L. & Song, J. H. Piezoelectric nanogenerators based on zinc oxide nanowire arrays. *Science* **312,** 242–246 (2006).
5. Chan, C. K. *et al.* High-performance lithium battery anodes using silicon nanowires. *Nature Nanotech.* **3,** 31–35 (2008).
6. McAlpine, M. C. *et al.* High-performance nanowire electronics and photonics on glass and plastic substrates. *Nano Lett.* **3,** 1531–1535 (2003).
7. Xu, F., Lu, W. & Zhu, Y. Controlled 3D buckling of silicon nanowires for stretchable electronics. *ACS Nano* **5,** 672–678 (2011).
8. Takei, K. *et al.* Nanowire active-matrix circuitry for low-voltage macroscale artificial skin. *Nature Mater.* **9,** 821–826 (2010).
9. Feng, X. L., He, R., Yang, P. & Roukes, M. L. Very high frequency silicon nanowire electromechanical resonators. *Nano Lett.* **7,** 1953–1959 (2007).
10. Park, H. S., Cai, W., Espinosa, H. D. & Huang, H. Mechanics of crystalline nanowires. *MRS Bull.* **34,** 178–183 (2009).
11. Richter, G. *et al.* Ultra high strength single crystalline nanowhiskers grown by physical vapor deposition. *Nano Lett.* **9,** 3048–3052 (2009).
12. Zhu, Y., Xu, F., Qin, Q. Q., Fung, W. Y. & Lu, W. Mechanical properties of vapor–liquid–solid synthesized silicon nanowires. *Nano Lett.* **9,** 3934–3939 (2009).
13. Chen, C. Q., Shi, Y., Zhang, Y. S., Zhu, J. & Yan, Y. J. Size dependence of the Young's modulus of ZnO nanowires. *Phys. Rev. Lett.* **96,** 75505 (2006).
14. Wu, B., Heidelberg, A. & Boland, J. J. Mechanical properties of ultrahigh-strength gold nanowires. *Nature Mater.* **4,** 525–529 (2005).
15. Chen, B. *et al.* Anelastic behavior in GaAs semiconductor nanowires. *Nano Lett.* **13,** 3169–3172 (2013).
16. Qin, Q. *et al.* Recoverable plasticity in penta-twinned metallic nanowires governed by dislocation nucleation and retraction. *Nature Commun.* **6,** 5983 (2015).
17. Zhu, Y. & Espinosa, H. D. An electromechanical material testing system for *in situ* electron microscopy and applications. *Proc. Natl Acad. Sci. USA* **102,** 14503–14508 (2005).
18. Chang, T. H. & Zhu, Y. A microelectromechanical system for thermomechanical testing of nanostructures. *Appl. Phys. Lett.* **103,** 263114 (2013).
19. Xu, F., Qin, Q. Q., Mishra, A., Gu, Y. & Zhu, Y. Mechanical properties of ZnO nanowires under different loading modes. *Nano Res.* **3,** 271–280 (2010).
20. Lifshitz, R. & Roukes, M. L. Themoelastic damping in micro- and nanomechanical systems. *Phys. Rev. B* **61,** 5600–5609 (2000).
21. Schaumann, G., Völki, J. & Alefeld, G. The diffusion coefficients of hydrogen and deuterium in vanadium, niobium, and tantalum by Gorsky-effect measurements. *Phys. Status Solidi* **42,** 401–413 (1970).
22. Schaumann, G., Völkl, J. & Alefeld, G. Relaxation process due to long-range diffusion of hydrogen and deuterium in niobium. *Phys. Rev. Lett.* **21,** 891–893 (1968).
23. McCluskey, M. D. & Jokela, S. J. Defects in ZnO. *J. Appl. Phys.* **106,** 071101 (2009).
24. Zhang, X., Kulik, J. & Dickey, E. C. Diffusion in Si_xGe_{1-x}/Si nanowire heterostructures. *J. Nanosci. Nanotechnol.* **7,** 717–720 (2007).
25. Zhu, T. & Li, J. Ultra-strength materials. *Prog. Mater. Sci.* **55,** 710–757 (2010).
26. Janotti, A. & Van de Walle, C. G. Native point defects in ZnO. *Phys. Rev. B* **76,** 165202 (2007).
27. Ashby, M. F. *Materials Selection in Mechanical Design* (Butterworth-Heinemann, 2010).
28. San Juan, J., Nó, M. L. & Schuh, C. A. Nanoscale shape-memory alloys for ultrahigh mechanical damping. *Nature Nanotech.* **4,** 415–419 (2009).
29. Perea, D. E. *et al.* Direct measurement of dopant distribution in an individual vapour–liquid–solid nanowire. *Nature Nanotech.* **4,** 315–319 (2009).
30. Wang, X. *et al.* Growth of uniformly aligned ZnO nanowire heterojunction arrays on GaN, AlN, and $Al_{0.5}Ga_{0.5}N$ substrates. *J. Am. Chem. Soc.* **127,** 7920–7923 (2005).

Acknowledgements

Y.Z. acknowledges support from the National Science Foundation (NSF) under awards CMMI-1030637 and 1301193, and the use of the Analytical Instrumentation Facility at North Carolina State University, which is supported by the State of North Carolina and the NSF. H.G. acknowledges support from the NSF through award CMMI-1161749 and the MRSEC Program through award DMR-0520651 at Brown University. C.M. acknowledges a scholarship from the China Scholarship Council (no. 2011683006). Y.Z. thanks Y. Gu and W. Lu for providing nanowire samples and for discussions about the defect structures in these nanowires.

Author contributions

Y.Z. conceived the idea. Y.Z. and H.G. designed the experiments and modelling. G.C., Q.Q. and F.X. performed the *in situ* mechanical testing. J.L., G.C. and E.C.D. performed EELS characterization. C.M. and H.H. performed the modelling and simulations. G.C., C.M., E.C.D., H.G. and Y.Z. wrote the paper. All authors discussed the results and commented on the manuscript.

Additional information

Supplementary information is available in the online version of the paper. Reprints and permissions information is available online at www.nature.com/reprints. Correspondence and requests for materials should be addressed to H.G. and Y.Z.

Competing financial interests

The authors declare no competing financial interests.

Methods

Synthesis of ZnO and Si nanowires. ZnO nanowires and Si nanowires were synthesized on Si/SiO_2 substrates using the vapour–liquid–solid (VLS) method, with Au colloids as catalysts. More details on nanowire synthesis are reported elsewhere[12,19].

***In situ* SEM testing.** A MEMS electrostatic actuator was used to bend an individual nanowire, which was clamped onto a nanomanipulator tip inside a SEM. The MEMS actuator, fabricated using a silicon-on-insulator process, was used for the bending tests[18]. Electrostatic actuation allowed the target displacement to be controlled precisely (on the order of 1 nm) and instantaneously (on the order of 1 μs), which is essential to monitor the relaxation and recovery processes in the present study. A nanomechanical testing system including a nanomanipulator (actuator) and an atomic force microscope cantilever (load sensor) was used for the tension and compression/buckling tests[19].

TEM, high-resolution TEM and STEM/EELS experiments. TEM and high-resolution TEM observations were performed for the ZnO nanowires on a JEOL 2010F operated at 200 kV. HAADF-STEM imaging and EELS quantitative analysis were carried out on an aberration-corrected FEI Titan 80–300 S/TEM with a Gatan EELS spectrometer operated at 200 kV. Details of the EELS analysis are provided in Supplementary Section 6.

Theoretical model. The nanowire was modelled as a beam with a hexagonal cross-section of diameter $2h$. The curvature κ of the nanowire can be related to the distributions of internal point defects as

$$\kappa = \kappa_e + \frac{16}{5\sqrt{3}h^4}\iint_D \sum_{i=1,2\cdots n} \frac{1}{3}\Omega_i c_i y \, \mathrm{d}x \, \mathrm{d}y \tag{1}$$

where subscripts $i \equiv 1, 2 \cdots n$ refer to all species of point defects, c_i and Ω_i are the concentrations and partial molar volume of the ith type of point defect, respectively, $\kappa_e = (16/5\sqrt{3}h^4)(M_e/E)$ is the elastic curvature caused by the applied external moment M_e, and E is Young's modulus. Considering diffusion of multiple types of internal point defects driven by gradients in their chemical potential, we derived the following governing equation:

$$\frac{\partial c_i}{\partial t} = D_i \frac{\partial}{\partial x}\left(\frac{\partial c_i}{\partial x} + \frac{1}{3}\frac{E\Omega_i c_i}{RT}\sum_{j=1,2\cdots n}\frac{1}{3}\Omega_j \frac{\partial c_j}{\partial x}\right) + D_i \frac{\partial}{\partial y}\left[\frac{\partial c_i}{\partial y} - \frac{1}{3}\frac{E\Omega_i c_i}{RT}\left(\kappa - \sum_{j=1,2\cdots n}\frac{1}{3}\Omega_j \frac{\partial c_j}{\partial x}\right)\right] \tag{2}$$

where D_i is the diffusion coefficient of the point defects, and R and T are the universal gas constant and temperature, respectively. More details of the model can be found in Supplementary Section 4.